Available online at www.sciencedirect.com
ScienceDirect
Ceramics International 37 (2011) 585–591
CERAMICS INTERNATIONAL
www.elsevier.com/locate/ceramint

Oxidation behavior of ZrB_2–$MoSi_2$–SiC composites in air at 1500 °C

Shuqi Guo [a,*], Takashi Mizuguchi [a], Masahide Ikegami [b], Yutaka Kagawa [a,b]

[a] Hybrid Materials Center, National Institute for Materials Science, 1-2-1 Sengen, Tsukuba, Ibaraki 305-0047, Japan
[b] Research Center for Advanced Science and Technology, The University of Tokyo, 4-6-1 Komaba, Meguro-ku, Tokyo 153-8904, Japan

Received 2 July 2010; received in revised form 20 August 2010; accepted 26 September 2010
Available online 28 October 2010

Abstract

We investigated the oxidation behavior and the effect of the amount of SiC added on oxidation resistance in both hot-pressed ZrB_2–$MoSi_2$–SiC composites, $55ZrB_2$–$40MoSi_2$–5SiC and $40ZrB_2$–$40MoSi_2$–20SiC (vol.%), exposed to dry air at 1500 °C for up to 10 h. Quantitative electron microprobe analysis characterizations of the chemical compounds of post-oxidized composites were carried out. Parabolic oxidation behavior was observed for both composites. The addition of SiC improved the oxidation resistance of ZrB_2–$MoSi_2$–SiC composites, and the improvement enhanced with amount of SiC added. The microstructure of the post-oxidized composites consisted of two characteristic regions: oxidized reactive region and unreactive bulk material region. The oxidized reactive region divided into an outermost dense silica-rich scale layer and oxidized reactive mixture layer. The improvement of oxidation resistance with SiC addition is associated with the presence of a thicker dense outermost scale layer which inhibited inward diffusion of oxygen through it.

Keywords: Ceramics; Corrosion; High-temperature properties; Electron microprobe analysis

1. Introduction

Zirconium diborides (ZrB_2)-based composites have become an important class of materials for structural applications at ultra high temperatures because they have an extremely high melting point (>3000 °C) [1–4]. A major problem with ZrB_2-based ceramics is high temperature oxidation where they are considered to be applied as structural materials for use in high-temperature oxidizing environments [5–7]. Heating ZrB_2 in air produces a scale composed of ZrO_2 and B_2O_3 in which B_2O_3 has a high vapor pressure and is vaporized above 1300 °C [5–7]. Thus, the oxidation resistance of ZrB_2 must be improved for use in oxidizing environments above 1300 °C.

To improve oxidation resistance, Si-containing additives, such as SiC and $MoSi_2$, are added to ZrB_2 [7–12], forming a protective borosilicate glass layer at temperatures above 1200 °C that enhances the oxidation resistance of ZrB_2. For the ZrB_2–SiC system, the main oxidation products are ZrO_2, B_2O_3, and SiO_2 below 1300 °C, ZrO_2 and SiO_2 above 1300 °C, as B_2O_3 liquid gets completely vaporized [5–10]. Generally, the resulting oxidized reactive region consists of three layers: (i) the outermost glassy layer, (ii) the oxide subsurface layer, and (iii) the SiC-depleted ZrB_2 layer. For the ZrB_2–$MoSi_2$ system, on the other hand, $MoSi_2$ is oxidized in atmospheric air, instead of SiC. Sciti et al. [11,12] examined the oxidation behavior of pressurelessly sintered 20 vol.% $MoSi_2$-containing ZrB_2 at 700–1400 °C in dry air. They showed that the oxidation resistance was improved with $MoSi_2$ added, as a result of formation of SiO_2 scale layer. The oxidation products consist of SiO_2, ZrO_2, $ZrSiO_4$, MoO_2, and MoB, and the oxidized reactive region consists of a SiO_2-rich glass layer; a subsurface oxide layer; and a MoB, ZrO_2, and SiO_2-containing mixture layer, depending on the exposure temperature. These studies demonstrated that the oxidized reactions of ZrB_2 depended on the composition, exposure temperature, and exposure time at a particular temperature, and oxygen content in the oxidizing atmosphere.

A recent study has shown that bending strength and fracture toughness are better for ZrB_2–$MoSi_2$–SiC system than for both ZrB_2–$MoSi_2$ system and ZrB_2–SiC system [13]. However, there is a little known of the oxidation behavior of ZrB_2–$MoSi_2$–SiC system. It could be expected that the oxidation behavior of the ZrB_2–$MoSi_2$–SiC system differs with both the ZrB_2–$MoSi_2$ and ZrB_2–SiC systems. In this study, two hot-pressed compacts of 5

* Corresponding author. Tel.: +81 029 859 2223; fax: +81 029 859 2401.
E-mail address: GUO.Shuqi@nims.go.jp (S. Guo).

0272-8842/$36.00
doi:10.1016/j.ceramint.2010.09.034

and 20 vol.% SiC-modified 40 vol.% $MoSi_2$-containing ZrB_2 were exposed in dry air at 1500 °C for up to 10 h. Quantitative characterization of the oxidized composites were conducted using electron probe micro analysis (EPMA) to identify the oxidation products, reactive compound composition, and their distribution. Also, the effect of amount of SiC added on oxidation behavior was examined.

2. Experimental

2.1. Oxidation test

The material used in this study was prepared by hot-pressing SiC-containing 40 vol.% $MoSi_2$–ZrB_2 composites. In order to examine the oxidation resistance of ZrB_2–$MoSi_2$–SiC composites as well as to learn the effect of amount of SiC added, two compositions of 5 and 20 vol.% SiC-modified 40 vol.% $MoSi_2$–ZrB_2 composites were hot-pressed at 1800 °C and 30 MPa in vacuum for 30 min. The detailed sintering process has been reported elsewhere [14]. Hereafter, the two compositions materials are denoted as ZMS5 and ZMS20.

Test specimens with average dimensions of 5 mm × 2.5 mm × 2 mm were cut from the hot-pressed ZrB_2–$MoSi_2$–SiC composites plates with a diamond wafered blade. After the specimens were polished with a diamond paste down to 1.0 μm, they were ultrasonically cleaned in acetone and then kept in an oven at a constant temperature of 100 °C prior to oxidation. Oxidation tests were performed using an electronic furnace (BFT-150-P, Nikkato Co., Ltd., Tokyo, Japan) at 1500 °C for up to 10 h in dry air. The heating and cooling rates were 20 °C and 10 °C/min, respectively. Before and after oxidation, the specimens were weighed, respectively, using an analytical balance (AB265-S, Mettler Toledo Co., Ltd., Switzerland) with an accuracy of 0.1 mg.

2.2. Characterization

X-ray diffraction (XRD) was used to identify major crystalline phases present in both the as-received and the post-oxidized composites. The oxidized surfaces were then characterized by scanning electron microscopy (SEM) and energy-dispersive X-ray spectroscopy (EDX). In order to examine the oxidation evolution, the oxidized specimens were cut in half, and one of the parts was mounted in epoxy and carefully polished with a diamond paste down to 1.0 μm. Cross-sectional observations of the oxidized sample's microstructures were conducted using a prototype wavelength dispersive-electron probe microanalyzer (WDS-EPMA) which was developed by Kimura et al. [15] based on a commercially available FE-EPMA (JEOL; JXA8900R). In addition, map analysis of O, C, Si, Mo, Zr, and B elements within the cross-section plane was conducted at 0.2 μm/step in the pixels of 200 × 1024 using an X-ray mapping technique with EPMA, with an accelerating voltage of 10 kV and probe current of 5.0×10^{-8} A. The X-ray image data obtained is projected on a two-dimensional space of X-ray intensity to form a histogram, which is generally called a scatter diagram. Detailed calculations of the scatter diagram have been reported elsewhere [16]. The analysis of the scatter diagram, i.e., the scatter diagram method, was used to identify the compounds composition as well as determine their distribution, with the pure SiO_2, ZrO_2, SiC, ZrB_2 and $MoSi_2$ powders as reference materials.

3. Results and discussion

3.1. Weight gain

In Fig. 1, the plots of weight gain as a function of exposure time for the composites are presented. The two compositions show similar oxidation behaviors: the specific weight increases rapidly within initial 1 h of exposure and then the weight increases gradually with exposure time, independent of the SiC amount. This suggests that the oxidation mechanism is the same for the two compositions. However, the weight gain was higher for ZMS5 than for ZMS20, showing the improvement of oxidation resistance with SiC added. Their specific weight gains are approximately 3 and 6 mg/cm^2, respectively, after 10 h of oxidation exposure. These gains are lower than those obtained in the 10–40 vol.% $MoSi_2$-containing ZrB_2 composites exposed at the same oxidation conditions which was previously reported by authors elsewhere [17].

Fig. 2 presents plots of the square of the weight gain, W^2, as a function of oxidation time, t, for the composites. The oxidation of the studied materials does not display parabolic kinetics at the initial stage of oxidation (within 1 h). The deviation from parabolic behavior suggests that the oxidation behavior of the studied materials is not appeared a parabolic behavior at the initial stage. After oxidation of 1 h, however, the parabolic behavior is observed for each curve. This suggests that after the outermost glassy scale formed at the initial stage of oxidation, the diffusion, such as outward diffusion of constituent elements from the bulk material to the oxidized region and the inward diffusion of oxygen through the scale layer, is the rate-controlling mechanism for oxidation, as observed for both ZrB_2–$MoSi_2$ and ZrB_2–SiC composites [9,10,12]. Similar oxidation behavior was previously reported in the 10–40 vol.%

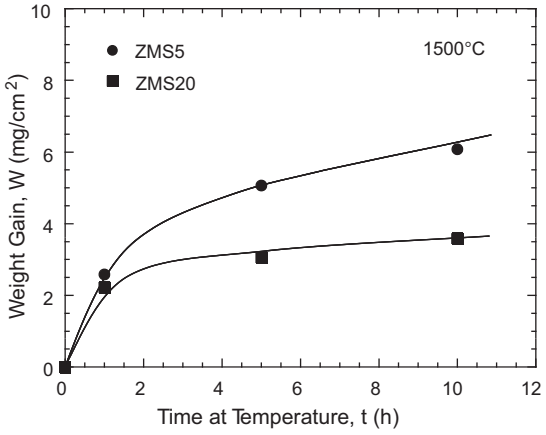

Fig. 1. Plots of weight gain as a function of exposure time for the ZrB_2–$MoSi_2$–SiC composites oxidized at 1500 °C.

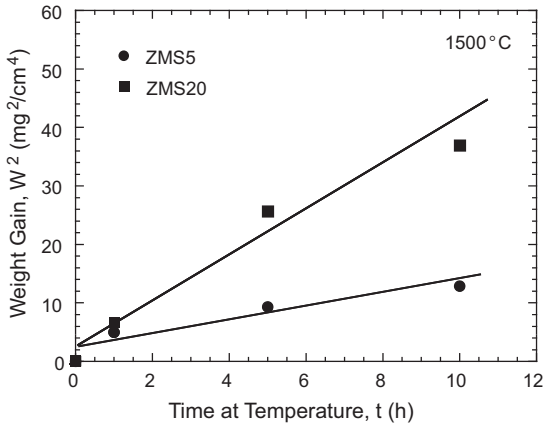

Fig. 2. Parabolic plots of specific weight gain as a function of time for the ZrB_2–$MoSi_2$–SiC composites oxidized at 1500 °C.

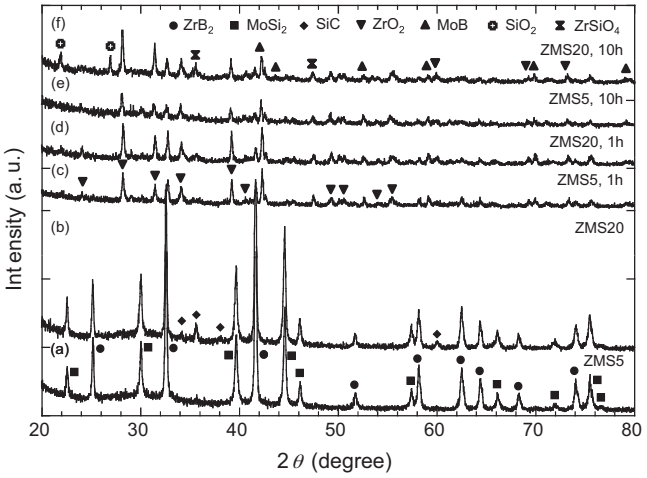

Fig. 3. X-ray diffraction patterns of the specimen surfaces for the ZrB_2–$MoSi_2$–SiC composites before and after oxidation exposure at 1500 °C for 1 h and 10 h: (a and b) pristine and (c–f) post-oxidized.

$MoSi_2$-containing ZrB_2 composites oxidized at the same oxidation condition [17]. To calculate parabolic rate constant of the studied materials, it is assumed that these materials follow the parabolic behavior for the period of 1–10 h. The parabolic oxidation rate constants of two compositions, obtained from the slopes of the straight lines, are ~3.6 and ~1.1 $mg^2\ cm^{-4}\ h^{-1}$ for ZMS5 and ZMS20, respectively. These values are lower than that (4.4 $mg^2\ cm^{-4}\ h^{-1}$) for SiC-free 40 vol.% $MoSi_2$-containing ZrB_2 composites oxidized at the same oxidation conditions [17]. Thus, the added SiC to ZrB_2–$MoSi_2$ system further improved its oxidation resistance, and the improvement is enhanced with increasing amount of SiC added.

3.2. Microstructure of oxidized samples

Fig. 3 shows XRD patterns of the two compositions before and after oxidation exposure. Before oxidation, only ZrB_2, $MoSi_2$ and SiC are detected for each composition. After oxidation, a new primary oxidized phase of ZrO_2 is detected in the two compositions. The minor oxidized phases of MoB and $ZrSiO_4$ phases were present as well. In addition, a trace of amount of SiO_2 phase was shown only in ZMS20. The intensity of ZrO_2 phase peaks decreases with the amount of SiC added, showing improved oxidation resistance, because of the ZrO_2 phase resulting from oxidation of ZrB_2. This agrees with the decrease in weight gain observed with increasing amount of SiC added (Fig. 1). For comparison, the intensity of ZrB_2 peaks is higher for the pristine samples than for the post-oxidized ones, indicating that those signals are from the bulk material beneath the scale layer. Additionally, the peak of $MoSi_2$ phase is absent in the both post-oxidized composites, a trace amount of SiC was detected only in the post-oxidized ZMS20. This indicates that SiC and $MoSi_2$ are thoroughly oxidized during the exposure. The crystalline phases identified in the as-sintered and post-oxidized samples are summarized in Table 1.

It is known that ZrB_2, $MoSi_2$ and SiC phases oxidize to form ZrO_2, B_2O_3, SiO_2 and MoB when ZrB_2–SiC and ZrB_2–$MoSi_2$ composites are exposed to air at high temperature. Previous studies in the ZrB_2–SiC composition show that ZrB_2 and SiC oxidize in air at 1500 °C, according to the following reactions [8,10]:

$$ZrB_2(s) + 2.5O_2(g) = ZrO_2(s) + B_2O_3(g) \quad (1)$$

$$SiC(s) + 1.5O_2(g) = SiO_2(s) + CO(g) \quad (2)$$

For the ZrB_2–$MoSi_2$ composition, on the other hand, ZrB_2 and $MoSi_2$ phases oxidize as they were exposed to air at high temperatures, according to the following reactions [12,17],

$$MoSi_2(s) + 3.5O_2(g) = MoO_3(g) + 2SiO_2(s) \quad (3)$$

$$ZrB_2(s) + 2MoSi_2(s) + 5O_2(g) = ZrO_2(s) + 2MoB(s) + 4SiO_2(s) \quad (4)$$

as a result of the outward diffusion of constituent elements cations from the bulk to the oxidized surface and the inward diffusion of O through the scale layer. In the present study, XRD analysis showed the presence of SiO_2, ZrO_2 and MoB phases in the post-oxidized samples (Fig. 3). The absence of B_2O_3 phase

Table 1
Crystalline phases in the pristine and oxidized ZrB_2–$MoSi_2$–SiC composites.

Materials		Before oxidation	After oxidation	
			1 h	10 h
ZMS5	Main phase	ZrB_2, $MoSi_2$	ZrO_2, ZrB_2	ZrO_2
	Minor phase	SiC	MoB, $ZrSiO_4$	ZrB_2, SiC, MoB, $ZrSiO_4$
ZMS20	Main phase	ZrB_2, $MoSi_2$	ZrO_2, ZrB_2	ZrO_2
	Minor phase	SiC	ZrB_2, MoB, $ZrSiO_4$	ZrB_2, SiC, MoB, $ZrSiO_4$, SiO_2

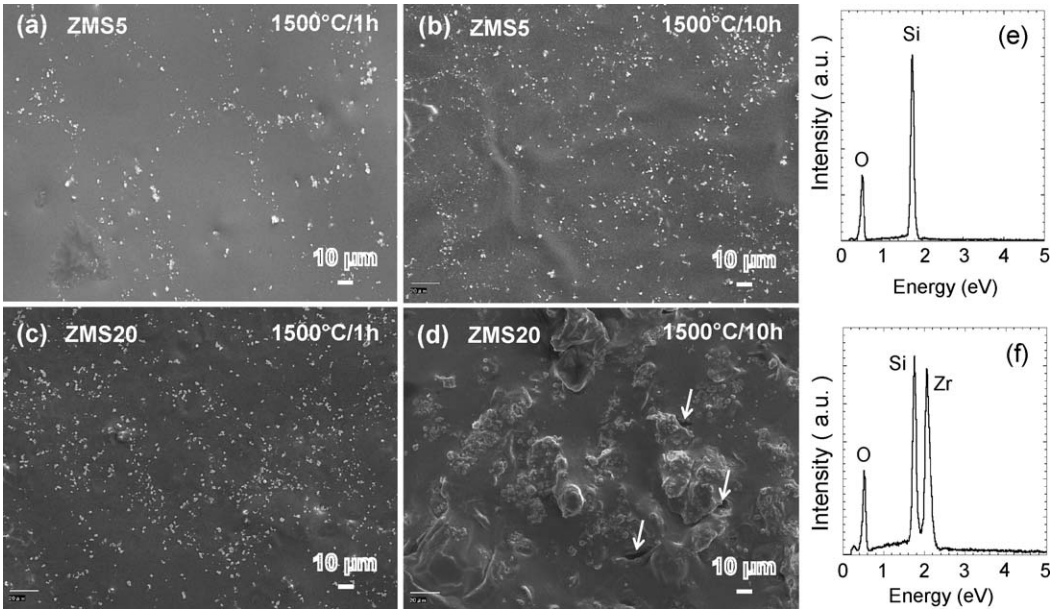

Fig. 4. Typical SEM images of the surface morphologies for the ZrB_2–$MoSi_2$–SiC composites oxidized at 1500 °C for 1 h (a and c) and 10 h (b and d), with EDX spectra of (e) background and (f) nodules particles.

is attributed to its vaporization above 1300 °C, as a result of its high vapor pressure. Thus, it could be expected that similar reactions occurred during the exposure at 1500 °C for the materials investigated in this study.

Thermodynamically, although the above-mentioned reactions are favored at high temperature, they did not occur simultaneously and their occurrence depended on exposure temperature. At 1500 °C, the reaction (1) has the more favorable followed by reaction (2), reactions (3) and (4) [18–20]. Thus, when the ZrB_2–$MoSi_2$–SiC composite was exposed to air at 1500 °C, the oxidation reaction conducted by the following sequence: (i) firstly ZrB_2 oxidized by air oxygen according to the reaction (1); (ii) then SiC oxidized according to the reaction (2); and (iii) finally $MoSi_2$ oxidized by the reactions (3) and (4). At the initial stage of exposure ZrB_2 firstly oxidized into ZrO_2 and B_2O_3, resulting in deviation of oxidation from parabolic behavior and the rapid increase of weight gain. Subsequently, SiC oxidized prior to $MoSi_2$ and a continuous and/or partially amorphous silica-rich glass scale was produced on the surface of samples. The formation of the scale, in particular continuous scale, inhibited the inward diffusion of oxygen in air, therefore improvement of oxidation resistance. Consequently, the oxidation behavior was controlled by inward diffusion of oxygen through the scale layer and outward diffusion of constituent elements cations from bulk materials. The later oxidation reaction of $MoSi_2$ accelerated the formation of the amorphous silica scale and increased the thick of the scale. Thus, it should be reasonable that the addition of SiC improved oxidation resistance of $MoSi_2$-containing ZrB_2 and this improvement was enhanced with increasing amount of SiC added. After ZrB_2, SiC and/or $MoSi_2$ oxidized, the ZrO_2 and amorphous silica coexisted in the silica-rich glass scale layer on the surface of samples. This results in a further reaction between ZrO_2 and amorphous silica. An early study [21] in ZrO_2 and amorphous silica showed that interstitial silicon diffuses and dissolves into crystalline ZrO_2 until the solution limit is reached when ZrO_2 and amorphous silica coexisted, thereafter precipitation of $ZrSiO_4$. In the present study, the peak of $ZrSiO_4$ was detected in the post-oxidized samples for both compositions materials. For comparison, crystalline SiO_2 was detected only in the ZMS20 sample oxidized for 10 h. The formation of crystalline SiO_2 is not well-understood but related with Si concentration in amorphous silica. It seems to expect the precipitation of crystalline SiO_2 from amorphous silica when Si concentration reached saturation.

Fig. 4 shows the typical surface morphologies for the two composites after oxidation. After oxidation of 1 h, the surfaces are covered with a continuous silica layer where white ZrO_2 particles of <1 μm diameter are embedded. For ZMS5, the ZrO_2 particles have not coarsened significantly even after oxidation of 10 h. For comparison, for ZMS20 after oxidation of 10 h the particles significantly coarsened to form the nodules. EDX analysis reveals that the background consists of only Si and O (Fig. 4(e)). This indicated that the background is an amorphous silicate phase for both the composites. This is similar to SiC-free ZrB_2–$MoSi_2$ composites oxidized under the same oxidation conditions [17]. For comparison, the nodules particles were oxide cluster where some larger ZrO_2 embedded in a SiO_2-rich glass matrix, verified by EDX analysis (Fig. 4(f)). In addition, some cracks are observed around the nodules (indicated by arrows in Fig. 4(d)). This cracking behavior is associated either with different thermal expansion between ZrO_2 and SiO_2 or with the volumetric change accompanying transformation of cristobalite from β- to α-phase as well as the phase transformation of tetragonal to monoclinic ZrO_2 on cooling [22,23].

In Fig. 5, the EPMA back-scattered images of the cross-section and corresponding X-ray image of various elemental

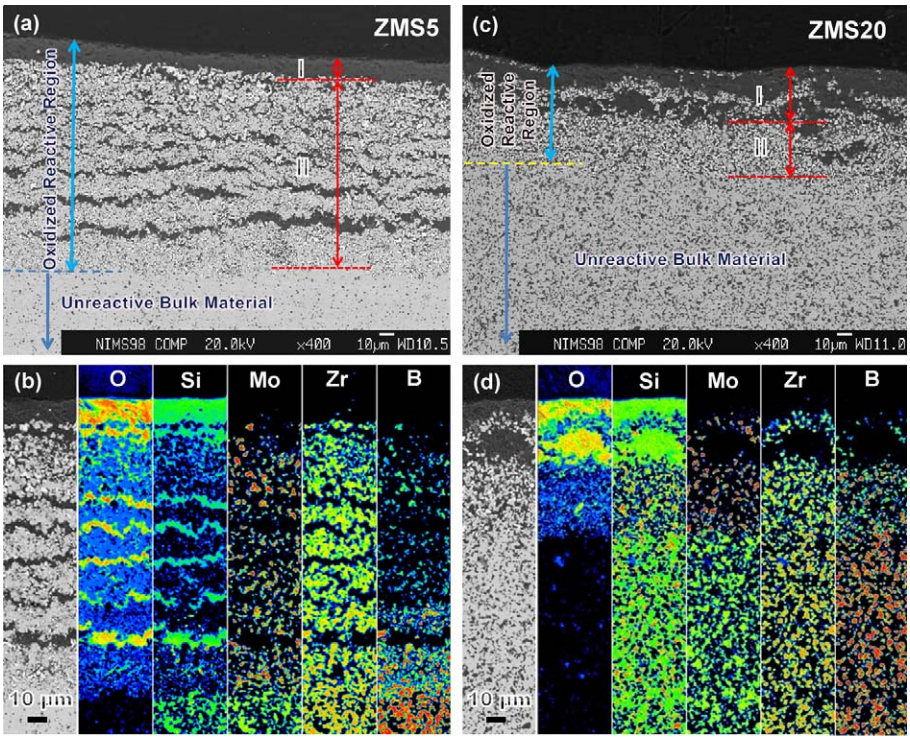

Fig. 5. Typical examples of EPMA backscattered image of the cross-section and elemental mappings under EPMA for (a and b) ZMS5 and (c and d) ZMS20 oxidized at 1500 °C for 10 h.

mappings of the composites oxidized for 10 h are presented. The cross-section of the post-oxidized samples is divided into the oxidized reactive region and the unreactive bulk material region. For ZMS5, the thickness of the reactive region is equal to ~148 μm which is almost the same with that of SiC-free 40 vol.% $MoSi_2$-containing ZrB_2 oxidized at 1500 °C for 10 h [17]. This reveals that 5 vol.% SiC added is significantly ineffective for further improving oxidation resistance of the ZrB_2–$MoSi_2$ composition. For ZMS20, the thickness of oxidized reactive region is equal to ~62 μm which is much thinner than that of ZMS5. Thus, 20 vol.% SiC added further significantly improved the oxidation resistance. In addition, the oxidized reactive region consists of two different characteristic layers, I and II. Layer I is a dense layer and it is rich Si and O (Fig. 5(b) and (d)). The thickness of layer I is much thicker than for ZMS20 than for ZMS5. This means that 20 vol.% SiC added formed a thicker dense scale layer which prevented effectively the inward diffusion of oxygen through it, therefore high oxidation resistance. Although the thickness of layer I in the studied materials is much thinner than for the SiC-free 40 vol.% $MoSi_2$-containing ZrB_2, the oxidation resistance is higher for the former than for the latter [17]. Obviously, this suggests that the oxidation resistance is not only linked with thickness of the scale layer, but also with its viscosity and compositions.

Moreover, layer II strongly depends on amount of SiC added, being much thicker for ZMS5 than for ZMS20. This suggests the layer I is more effective for inhibiting inward diffusion of oxygen during exposure for ZMS20 than for ZMS5. This is associated with the presence of some crystalline SiO_2 phase in it because layer I contains some crystalline SiO_2 phase for ZMS20 but the absence of crystalline SiO_2 phase for ZMS5, with a thicker dense layer I for the former as well. Layer II is very complex and it contains O, Si, Mo, Zr and B. The morphology of layer II is strongly dependent on the amount of SiC added. For ZMS5, it is found layer upon layer of layer II which is stacked by (Si, O)-rich layer and (Mo, Zr, B)-rich layer. A similar structure was previously reported in 40 vol.% $MoSi_2$-containing ZrB_2 oxidized at 1500 °C for 10 h [17]. For comparison, in the case of ZMS20, layer II consists of a single layer. The unreactive bulk material region contains Si, Mo, Zr, C and B, but no O. Hence, the unreactive bulk material consists of Zr–B, Mo–Si and Si–C phases.

3.3. Compositions and distribution of reactive compounds

Fig. 6 shows the detailed oxidation products distribution and compositions in the cross-section for the composites oxidized for 10 h, with the scatter diagram method under EPMA. The Si–O phase is the major reactive compound in layer I for the two compositions, and a trace amount of Zr–O and M–B phases is present in it as well. Layer II has the complex compounds and it consists of Si–O, Mo–B, Zr–O, and Si–C, Zr–B phases. For ZMS5, layer II is divided into two sublayers: II(a) and II(b). Sublayer II(a) consists of Si–O, Mo–B, and Zr–O phases in which Zr–O is the primary phase, while SiC, ZrB_2 and $MoSi_2$ were not shown. In sublayer II(b), the Zr–B phase and a trace amount of Si–C phase are also present, but the Mo–Si phase is absent in the both layers. Differing from ZMS5, in ZMS20 sublayer II(a) is absent, only sublayer II(b) is observed. In sublayer II(b), the Zr–O, Mo–B and SiC phases are present, and

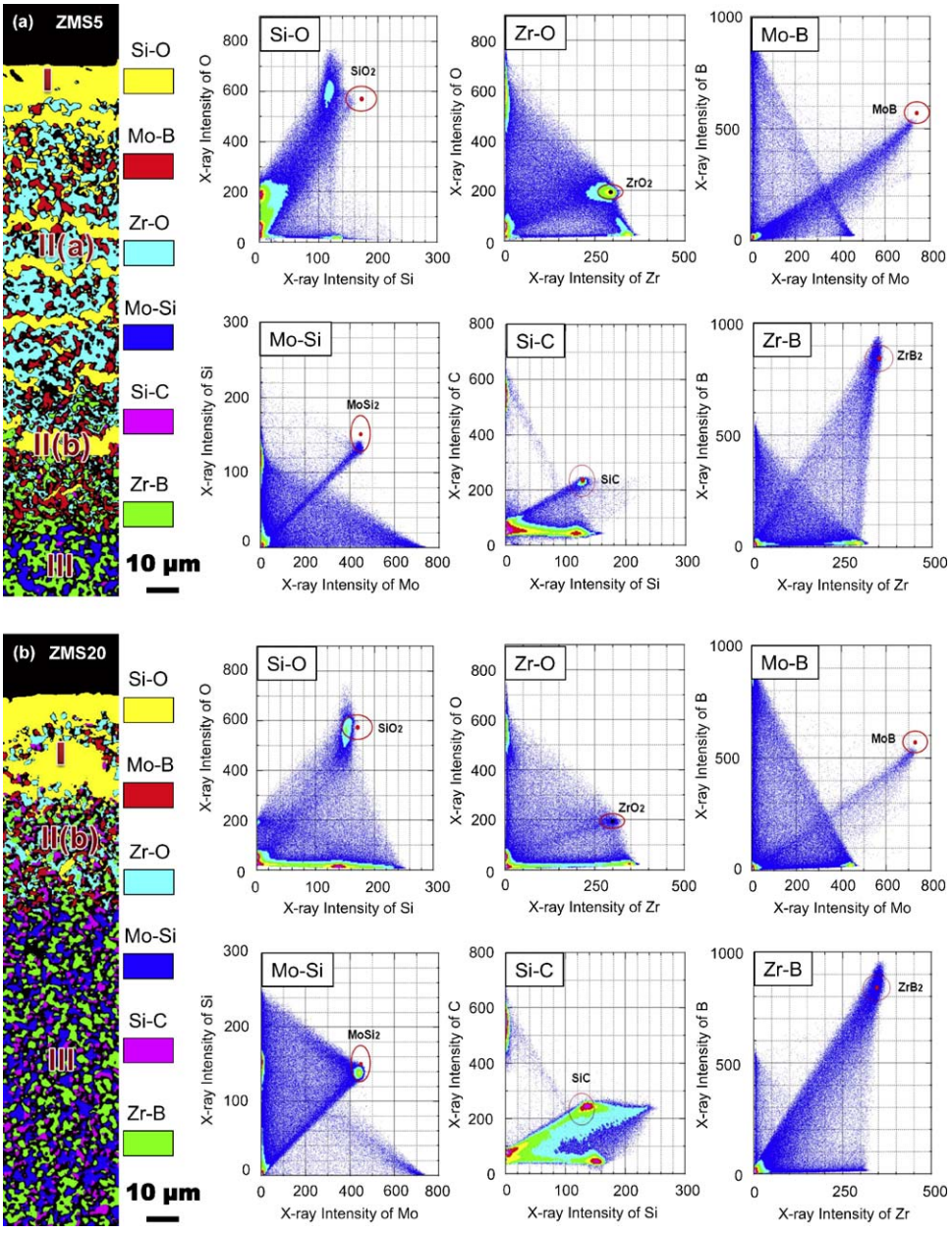

Fig. 6. Examples of X-ray images of phase mapping of the cross-section under EPMA and the scatter diagrams of Si *vs.* O, Zr *vs.* O, Mo *vs.* B, Mo *vs.* Si, Si *vs.* C and Zr *vs.* B for (a) ZMS5 and (b) ZMS20 oxidized at 1500 °C for 10 h.

a trace amount of Si–O phase is present as well. Thus, layer II is a SiC- and $MoSi_2$-depleted zone where the oxidation reaction occurred, and it is more extended for ZMS5, compared to ZMS20. Hence, the addition of SiC promoted formation of thicker dense glassy scale on the surface of samples which inhibited effectively outward diffusion of oxygen through it, therefore improving oxidation resistance. The unreactive bulk material region is the same for the two compositions and it consists of Zr–B, Mo–Si and Si–C phases.

In order to identify the reactive compound compositions as well as to examine a change of the chemical compounds during exposure, the analysis of X-ray image data for Si, O, Zr, Mo, C and B elements is conducted on the cross-section. The scatter diagrams of the obtained characteristic X-ray intensities for Si–O, Zr–O, Mo–B, Mo–Si, Si–C, and Zr–B phases are also shown in Fig. 6, in which each point represents the number of the same intensities. Note that the solid circle in each figure represents the pure stoichiometric SiO_2, ZrO_2, $MoSi_2$, SiC, and ZrB_2 phases. It is found that the crystalline Zr–O, M–B, Mo–Si, Si–C and Zr–B phases are the stoichiometric ZrO_2, MoB, $MoSi_2$, SiC and ZrB_2 phases for both compositions. On the other hand, for ZMS5 the composition of amorphous Si–O phase is determined to be 33.2 mass.% Si and 52.0 mass.% O, deviating from the pure SiO_2 phase of 46.74 mass.% Si and 53.26 mass.% O. This means that Si is depleted in outermost amorphous scale, as a result of diffusion and dissolution of Si into ZrO_2 [21]. Similar

behavior was previously reported in SiC-free 40 vol.% $MoSi_2$-containing ZrB_2 composites [17]. Differing with the previous study, the nonstoichiometric $MoSi_2$ was not detected in this study. This shows that although 5 vol.% SiC added is ineffective for significantly improving oxidation resistance of 40 vol.% $MoSi_2$-containing ZrB_2, but inhibiting oxidation of $MoSi_2$ in the unreactive bulk materials. For comparison, for ZMS20 the Si–O phase is determined to be 41.9 mass.% Si and 53.8 mass.% O, being close with a pure SiO_2 phase. This suggests that 20 vol.% SiC added supplies amount of Si needed for forming a pure SiO_2 phase. Based on the above-mentioned amorphous silica phase composition, it seems to be expected that the crystalline SiO_2 phase in ZMS20 precipitated from the amorphous silica phase which composition was close to pure SiO_2 on cooling, as a result of saturation of Si concentration. In addition, analysis of the scatter diagrams of Zr–B, Mo–Si and Si–C shows that these compounds are stoichiometric. Previous study of ZrB_2–$MoSi_2$ shows that Mo–Si phase is nonstoichiometric $MoSi_2$, as a result of the outward diffusion of Si during exposure. Thus, the addition of SiC seems to be effective for supplying enough Si source for precipitating a crystalline SiO_2 phase from amorphous silica as well as increasing viscosity of the amorphous silica-rich glass scale layer, therefore inhibiting the outward diffusion of Si from the unreactive bulk and the inward diffusion of oxygen through the scale layer during oxidation exposure.

4. Conclusions

In conclusion, the oxidation resistance of the ZrB_2–$MoSi_2$–SiC composites is improved with SiC addition, and the improvement enhanced with amount of SiC added. The microstructure of the oxidized ZrB_2–$MoSi_2$–SiC composites consists of an outermost dense glassy scale, middle oxidized reactive layer, and an unreactive bulk material. The outermost dense scale layer is much thicker for ZMS20 than for ZMS5. However, the middle oxidized reactive layer is much greater for ZMS5 than for ZMS20. The dense scale layer consists of ZrO_2 and amorphous silica where ZrO_2 embedded in SiO_2-rich glass matrix, a trace amount of MoB and $ZrSiO_4$ was presented. For ZMS20, a crystalline SiO_2 phase was also present in the post-oxidized sample for 10 h, with a trace amount of SiC. The middle reactive layer is composed of complex compounds, and it consisted of amorphous SiO_2-rich glass, crystalline ZrO_2, MoB, SiC and ZrB_2 for both compositions. The unreactive bulk material is the same for both compositions composites, consisting of ZrB_2, $MoSi_2$, and SiC.

Acknowledgements

The authors would like to thank Dr. T. Kimura and Mr. T. Aoyagi, National Institute for Materials Science, for his assistance with EPMA measurements as well as discussion.

References

[1] C. Mroz, Zirconium diboride, Am. Ceram. Soc. Bull. 73 (1994) 141–142.
[2] K. Upadhya, J.M. Yang, W.P. Hoffmann, Materials for ultrahigh temperature structural applications, Am. Ceram. Soc. Bull. 76 (1997) 51–56.
[3] A.S. Brown, Hypersonic designs with a sharp edge, Aerospace Am. 35 (1997) 20–21.
[4] S. Norasetthekul, P.T. Eubank, W.L. Bradley, B. Bozkurt, B. Stucker, Use of zirconium diboride-copper as an electrode in plasma applications, J. Mater. Sci. 34 (1991) 261–270.
[5] A.K. Kuriakose, J.L. Margrave, Oxidation kinetics of zirconium diboride and zirconium carbides at high temperatures, J. Electrochem. Soc. 111 (1964) 827–831.
[6] J.B. Berkowitz-Mattuck, High temperature oxidation, J. Electrochem. Soc. 113 (1966) 908–914.
[7] W.C. Tripp, H.H. Davis, H.C. Graham, Effect of an SiC addition on the oxidation of ZrB_2, Am. Ceram. Soc. Bull. 52 (1973) 612–616.
[8] F. Monteverde, A. Bellosi, Oxidation of ZrB_2-based ceramics in dry air, J. Electrochem. Soc. 150 (2003) B552–B559.
[9] W.G. Fahrenholtz, Thermodynamic analysis of ZrB_2–SiC oxidation: formation of a SiC-depleted region, J. Am. Ceram. Soc. 90 (2007) 143–148.
[10] A. Rezaie, W.G. Fahrenholtz, G.E. Hilmas, Evolution of structure during the oxidation of zirconium diboride–silicon carbide in air up to 1500 °C, J. Eur. Ceram. Soc. 27 (2007) 2495–2501.
[11] D. Sciti, M. Brach, A. Bellosi, Long-term oxidation behavior and mechanical strength degradation of a pressurelessly sintered ZrB_2–$MoSi_2$ ceramic, Scripta Mater. 53 (2005) 1297–1302.
[12] D. Sciti, M. Brach, A. Bellosi, Oxidation behavior of a pressureless sintered ZrB_2–$MoSi_2$ ceramic composite, J. Mater. Res. 20 (2005) 922–930.
[13] S.Q. Guo, T. Nishimura, T. Mizuguchi, Y. Kagawa, Mechanical properties of hot-pressed ZrB_2–$MoSi_2$–SiC composites, J. Eur. Ceram. Soc. 28 (2008) 1891–1898.
[14] S.Q. Guo, T. Nishimura, H. Tanaka, Y. Kagawa, Thermal and electrical properties in hot-pressed ZrB_2–$MoSi_2$–SiC composites, J. Am. Ceram. Soc. 90 (2007) 2255–2258.
[15] T. Kimura, K. Nishida, S. Tanuma, Spatial resolution of a wavelength-dispersive electron probe microanalyzer equipped with a thermal field emission gun, Microchim. Acta 155 (2006) 175–178.
[16] T. Kimura, T. Sugizaki, K. Nishida, N. Ishikawa, S. Tanuma, Analysis of joining boundary between Ni–P Electroless plate and solder by EPMA scatter diagram method, J. Jpn Inst. Metals. 68 (2004) 8–13.
[17] S.Q. Guo, T. Mizuguchi, T. Aoyagi, T. Kimura, Y. Kagawa, Quantitative electron microprobe characterizations of oxidized ZrB_2 containing $MoSi_2$ additives, Oxid. Metals 72 (2009) 335–345.
[18] W.G. Fahrenholtz, G.E. Hilmas, I.G. Talmy, J.A. Zaykoski, Refractory diborides of zirconium and hafnium, J. Am. Ceram. Soc. 90 (2007) 1347–1364.
[19] Z.H. Yang, D.C. Jia, Y. Zhou, P.Y. Shi, C.B. Song, L. Lin, Oxidation resistance of hot-pressed SiC–BN composites, Ceram. Int. 34 (2) (2008) 317–321.
[20] Y.Q. Liu, G. Shao, P. Tsakiropoulos, On the oxidation behavior of $MoSi_2$, Intermetallics 9 (2) (2001) 125–136.
[21] C. Veytizou, J.F. Quinson, O. Valfort, G. Thomas, Zircon formation from amorphous silica and tetragonal zirconia: kinetic study and modeling, Solid State Ionics 139 (2001) 315–323.
[22] D.M. Mieskowski, W.A. Sanders, Oxidation of silicon nitride sintered with rare-earth oxide additives, J. Am. Ceram. Soc. 68 (1985) C160–163.
[23] M.H. Bocanegra-Bernal, S. Diaz De La Torre, Review: phase transitions in zirconium dioxide and related materials for high performance engineering ceramics, J. Mater. Sci. 37 (2002) 4947–4971.